Original paper

Folia Neuropathologica

Impact of inflammation-related degenerative changes on the wall strength of unruptured intracranial aneurysms: a pilot study

Leszek Lombarski[1], Przemysław Kunert[1], Sylwia Tarka[2], Tomasz Stępień[3], Dominik Chutorański[3], Sławomir Kujawski[4], Andrzej Marchel[1]

[1]Department of Neurosurgery, Medical University of Warsaw, Warsaw, Poland, [2]Department of Forensic Medicine, Medical University of Warsaw, Warsaw, Poland, [3]Department of Neuropathology, Institute of Psychiatry and Neurology, Warsaw, Poland, [4]Department of Exercise Physiology and Functional Anatomy, Collegium Medicum in Bydgoszcz, Nicolaus Copernicus University in Toruń, Bydgoszcz, Poland

Folia Neuropathol 2022; 60 (4): 403-413 *DOI: https://doi.org/10.5114/fn.2022.122342*

Abstract

Introduction: *Saccular intracranial aneurysm (sIA) rupture is a serious cerebrovascular event associated with inflammatory destructive processes leading to gradual weakening of the sIA wall. The aim of the present study was to identify the morphological and histological determinants for low wall strength in unruptured sIAs harvested from autopsy subjects.*
Material and methods: *A total of eight single unruptured sIAs were identified and excised with adjacent cerebral arteries during 8 of 184 postmortem examinations. The dome morphology was assessed for each sIA at a constant pressure of 100 mmHg. Then, after 5 preconditioning cycles which assured muscle fibre relaxation, sIA specimens were subjected to gradually increasing intraluminal pressure at a rate of 20 mmHg/s until rupture of the sIA or cerebral artery was achieved. Micro-structural degenerative changes and inflammatory cell infiltration within the sIA wall were quantitatively analysed after pressurization of the sIA specimens. The microscopic analysis of the slides stained with histological methods (HE, Mallory trichrome, Masson trichrome, orcein) and immunohistochemical methods (LCA, CD3, CD68) was performed.*
Results: *The wall of the sIA ruptured in three specimens, while in the other cases, rupture occurred at the arterial wall. The mean maximal dome size was significantly larger in sIAs with low wall strength, that is, in sIAs that ruptured during pressurization, than in sIAs with high wall strength (6.46 mm vs. 2.43 mm, p = 0.034). Moreover, a significantly higher average percentage of wall hyalinization in sIAs that ruptured than in sIAs that did not rupture was observed (30% vs. 0%, p = 0.006). In contrast, the degree of inflammatory cell infiltration did not differ between the wall strength categories.*
Conclusions*: Our results support the observations that larger sIAs may be at a higher risk of rupture. Histological analysis revealed that hyalinization corresponds to the weakened regions of the wall of unruptured sIAs.*

Key words: *inflammation, rupture risk, saccular intracranial aneurysm, aneurysm morphology, rupture pressure, hyalinization.*

Introduction

Due to recent advances in brain imaging, unruptured saccular intracranial aneurysms (sIAs) are being increasingly diagnosed, with an estimated incidence of 3% in the general population. Most incidentally detected unruptured sIAs are small, with diameters < 5 mm [13], and are characterized by a very low risk of future bleeding [6]. However, up to 47% of ruptured sIAs presenting with subarachnoid haemorrhage are < 5 mm in size [12]. In addition, subarachnoid haemorrhage is

Communicating author:
Sylwia Tarka, PhD, Department of Forensic Medicine, Medical University of Warsaw, Warsaw, Poland, e-mail: sylwia.tarka@wum.edu.pl

associated with a high fatality rate [2,6,19]. Nevertheless, the only available preventive methods utilize invasive procedures with a combined morbidity and mortality rate reaching 10.1% [1]. To determine which group of patients harbouring unruptured sIAs may benefit from such treatment, diagnostic tools facilitating identification of rupture-prone sIAs should be developed.

Aneurysms are often located within the bifurcation of the vessels, which may be a manifestation of developmental disorders arising in the very early stage of ontogenesis. Disturbances in the processes of migration and differentiation of cells derived from two germ laminae may cause underdevelopment of arterial bifurcation and the formation of anomalies at the bifurcation site [18]. According to mathematical models, some sIAs may rupture soon after formation [22] however, most sIAs are characterized by irregular growth with an increased or decreased risk of subarachnoid haemorrhage occurring interchangeably [9]. Particular hemodynamic conditions are hypothesized to be responsible for both healing and destructive processes associated with inflammation of the sIA wall. Therefore, sIAs rupture when destructive processes predominate irrespective of the dome size [14]. Furthermore, histological data from studies comparing ruptured and unruptured sIAs demonstrated marked differences in decellularization, wall matrix degradation and the degree of inflammatory cell infiltration within the aneurysmal wall [4,8,16]. However, the limitation of directly comparing ruptured and unruptured sIAs is the inability to evaluate the exact effect of the rupture event on the influx of inflammatory cells.

Recent studies concerning biomechanical features of unruptured sIAs revealed differences in mechanical behaviour during uniaxial extension tests between sIAs characterized by low and high wall strength. Nevertheless, these biomechanical studies refer exclusively to a sample of sIA dome collected during surgery and do not consider complexity of the sIA wall structure [21]. The aim of the present study was to determine whether morphological features, microstructural degenerative changes and inflammatory cell infiltration play a role as potential indicators of the low wall strength in the intact specimens of unruptured sIAs.

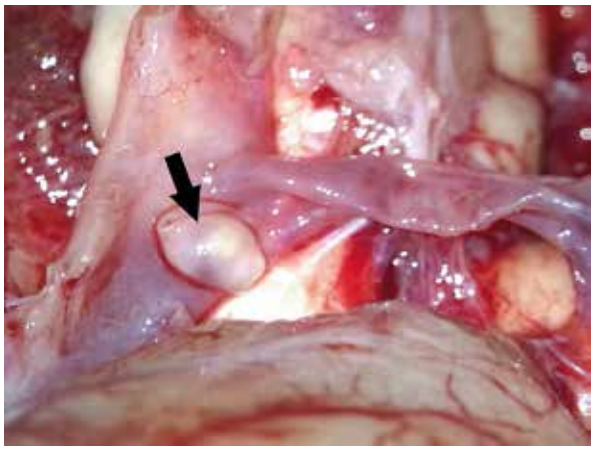

Fig. 1. Unruptured aneurysm (arrow), surgical microscope view.

Material and methods

Aneurysm specimens

During consecutive forensic autopsies, a total of 184 brains obtained from cadavers of individuals who died from extracerebral causes were studied (age 60 ±8 years, 53 females). Prior to the autopsies, the cadavers were stored at 4°C. The period between the time of death and autopsy did not exceed 36 hours. Eight single unruptured sIAs were identified among 8 cadavers (age 62 ±4 years, 2 females). Following stepwise dissection of the subarachnoid cisterns, the sIAs with adjacent parent arteries and their main branches were excised using a surgical microscope (Carl Zeiss OPMI pico S100, Germany) (Fig. 1). All experiments were performed in accordance with relevant guidelines and regulations. The approval of the local ethics committee and the informed consent obtained from the family member were not required for the use of autopsy material in the present study.

Morphometry and pressure-inflation tests

Pressure-inflation tests were performed in a working area specifically designed by engineers from the Warsaw University of Technology supported by funds from the Dean's Grant from September 2011 to March 2012 (Fig. 2). The pressure was measured using a pressure sensor with a performance range of 0-4560 mmHg, output signal of 0-10 V and error < 0.1%. Blood clots were rinsed with 0.9% NaCl immediately after extraction. Once the specimen was inserted onto a flared tip cannula, it was sealed by ligating its perforators and both ends. Then, a precision dosing pump was activated to deliver 0.9% NaCl at 36°C. The presence of dome irregularity was assessed. The neck width and maximal dome size of each sIA were measured at a pressure of 100 mmHg to reflect the in vivo size (Fig. 2). Prior to the pressure-inflation test, 5 preconditioning cycles were performed with gradually increasing and decreasing pressures ranging from 0 to 200 mmHg (10 mmHg/s) to induce muscle fibre relaxation. Next, the specimen was subjected to a quasi-static increasing pressure (20 mmHg/s). Pressure application and visual registration were continued until rupture of the sIA wall, parent artery or one of its branches (Fig. 2). sIAs were classified into the low-wall strength category when the sIA dome

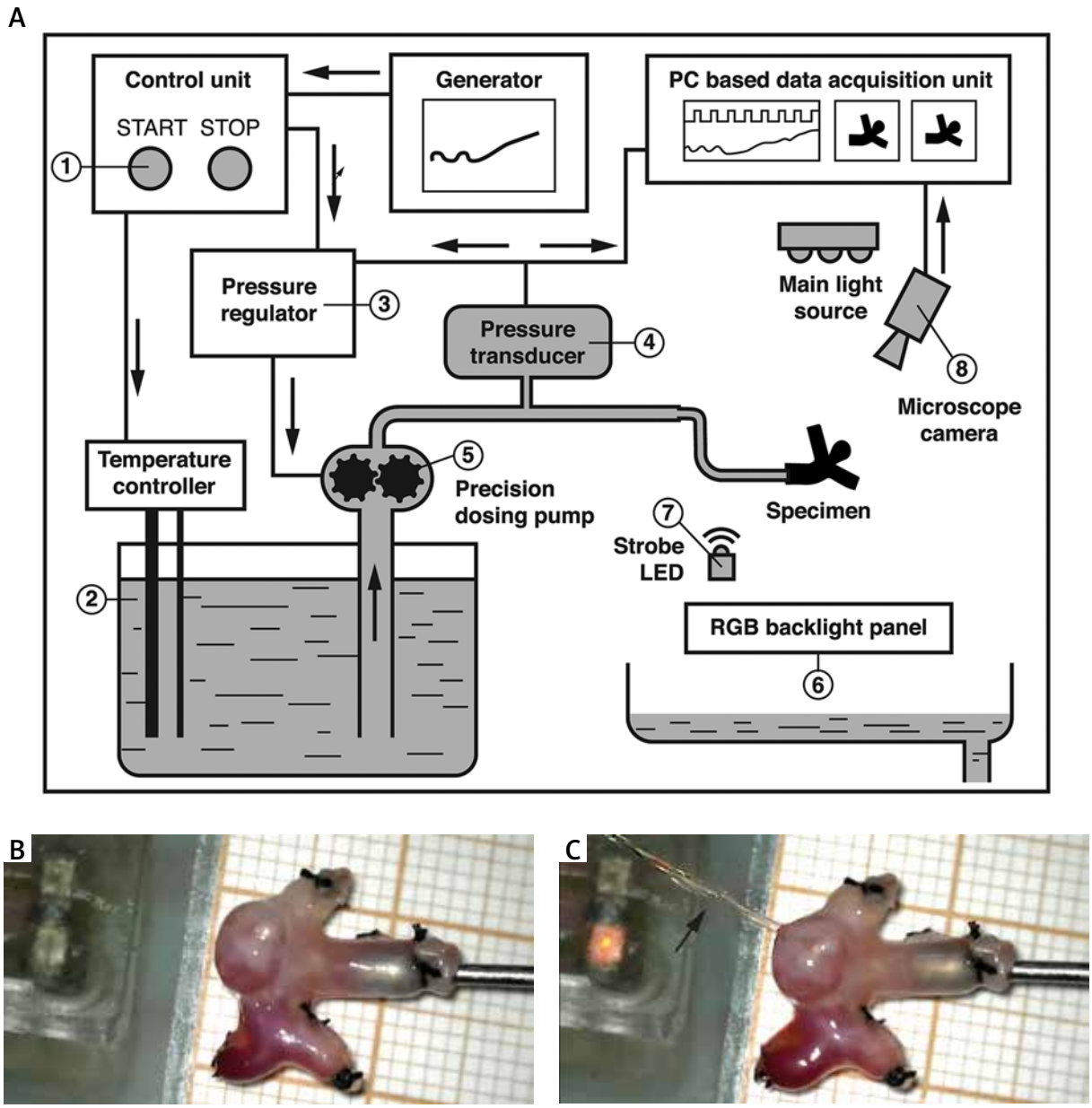

Fig. 2. Pressure-inflation tests. **A**) Block diagram of the working area. Following activation (1), the temperature controller regulates the temperature of 0.9% NaCl (2), maintaining its predefined value and transmitting a specified pressure to the pressure regulator (3). Because of the feedback signal from the pressure transducer, (4) the regulator maintains proper pressure within the analysed sIA specimen by controlling the precision dosing pump (5). Multicolour lights (6) provide optimal conditions for visual registration. LED diodes (7) correlate the pressure with the image from the camera (8). **B**) Unruptured left middle cerebral artery bifurcation sIA mounted on the flared tip cannula and pressurized to 100 mmHg. **C**) The same sIA at the moment of rupture; the black arrow indicates the stream of 0.9% NaCl.

ruptured and the high-wall strength category when the rupture occurred at the adjacent cerebral artery. The follow-up steering control system regulated the pump revolutions to provide a constant increase in pressure. The obtained sIA morphological characteristics and rupture pressure values of the analysed specimens were compared depending on the sIA wall strength category.

Fig. 3. Irregular intracranial aneurysm with a thickened wall. Magnification 40×, Masson-Goldner trichrome stain.

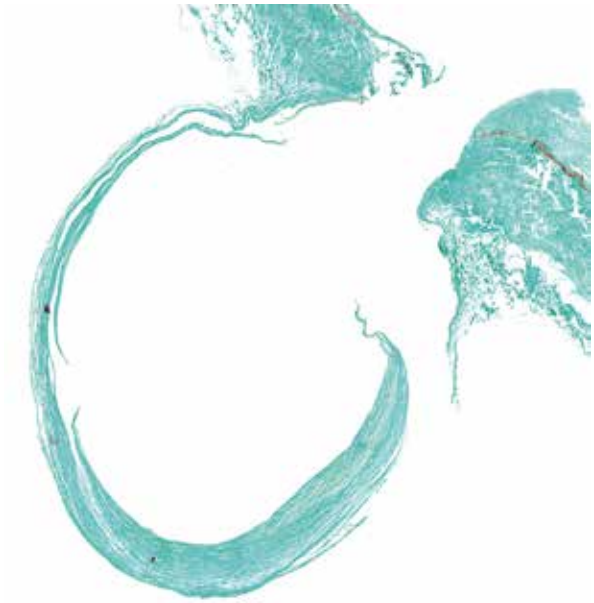

Fig. 5. Small regular intracranial aneurysm with a thickened wall. Magnification 40×, Masson-Goldner trichrome stain.

Histological and immunohistochemical analyses

Specimens were fixed in 4% buffered formalin and then embedded in paraffin blocks along the long axis of the parent artery to cover the dome and neck of the sIA during serial cutting for 5-µm sections. The sections were stained with haematoxylin-eosin and Masson-Goldner trichrome, Mallory trichrome, orcein. Then, the sIAs were studied under a microscope (Olympus BX53, Japan) by one of the investigators

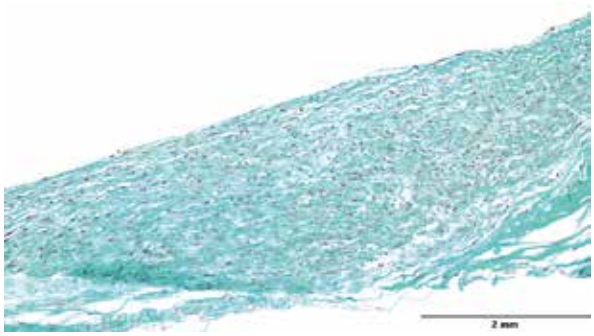

Fig. 4. Aneurysm wall with disorganized smooth muscle cells. Magnification 200×, Masson-Goldner trichrome stain.

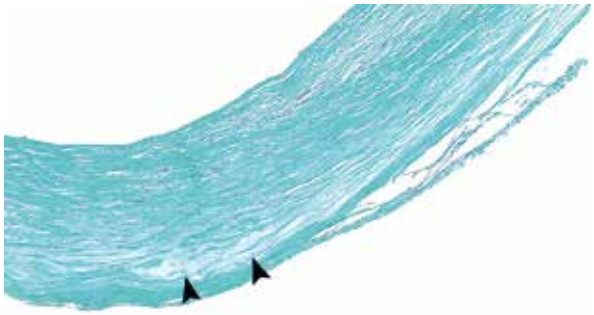

Fig. 6. Aneurysm wall with myointimal hyperplasia and region of hyalinization (arrows). Magnification 200×, Masson-Goldner trichrome stain.

who remained blinded to the rupture site. Degradation of the internal elastic lamina (IEL) was analysed qualitatively. Degenerative changes in the sIA wall were evaluated based on the classification of histological wall types of sIAs presented by Frösen *et al.* reflecting gradual progression of wall degeneration: type A – an endothelium covered wall with linearly organized smooth muscle cells; type B – a thickened wall with disorganized smooth muscle cells (Figs. 3, 4); type C – a hypocellular wall with myointimal hyperplasia or organized luminal thrombosis (Figs. 5, 6); and type D – an extremely thin and thrombosis-lined hypocellular wall (Figs. 7, 8) [4]. Having considered the differences in the methodology and the type of material used for microscopic analysis, the presence of thrombus and endothelium was not included. In another study regarding the aneurysmal wall structure of both ruptured and unruptured sIAs, Kataoka et al. included the presence of hyalinization in their histological comparative analysis. Since hyalinised tissue was present within the wall of

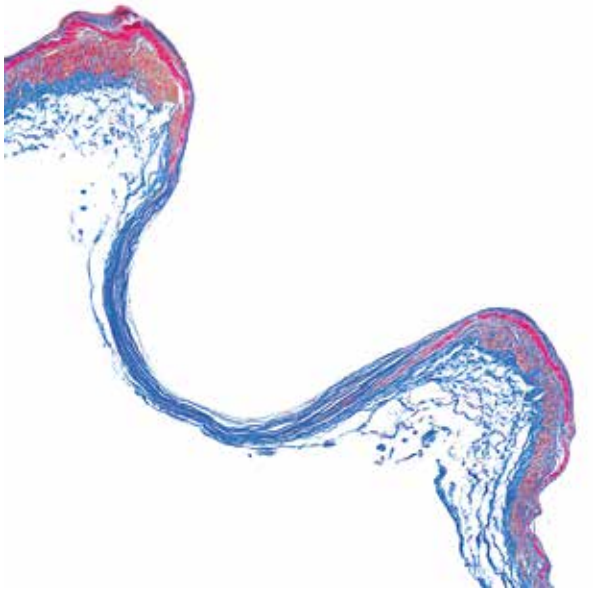

Fig. 7. Small regular thin-walled aneurysm. Magnification 100×, Mallory trichrome stain.

ruptured sIAs [8], we distinguished an additional type E corresponding to the regions of wall hyalinization (Fig. 6). The average percentages of different types of degenerative changes in the sIA wall were assessed on 3 representative sections.

Immunohistochemistry was conducted using the mouse monoclonal antibodies anti-LCA (Dako, 8B11-PD7/26, 1 : 75), anti-CD3 (Dako-Agilent, clone F7.2.38, 1 : 50) and anti-CD68 (Cell Marque-Sigma Aldrich, clone Kp-1, 1 : 250). The epitopes were exposed thermally (HIER – heat-induced epitope retrieval) by heating in citrate buffer (pH = 6, microwave 3 × 5 minutes). This was followed by blocking endogenous peroxidases with 1% TRIS + H_2O_2 (Tris Base T1503, pH = 7.6) for 20 minutes and rinsing in TRIS for 10 minutes. Subsequently, the sections were outlined and incubated in horse serum for 1 hour (Vector Laboratories S-2000 Normal Horse Serum) and then with the primary antibodies (12 hours, 4°C). A universal system by Vector (PK-7200) was used for detection. Visualization was performed using diaminobenzidine (DAB) (Sigma Aldrich). We identified T cells and macrophages, because according to Frösen ones are the best predictors of aneurysm rupture [4]. The degree of inflammatory cell infiltration was determined quantitatively by estimating the number of T lymphocytes ($CD3^+$) and macrophages ($CD68^+$) per standardized grid area (0.0625 mm^2 at 40× magnification) [4] in 2 areas of the sIA dome with the most robust inflammation in particular layers of its wall. The average density of inflammatory cell infiltration was calculated separately for T lymphocytes and macrophages within the adventitia and inner layers of the sIA wall. The percentages of different types of degenerative changes and the density of inflammatory cell infiltration in particular sIA wall layers were compared with respect to the sIA wall strength category.

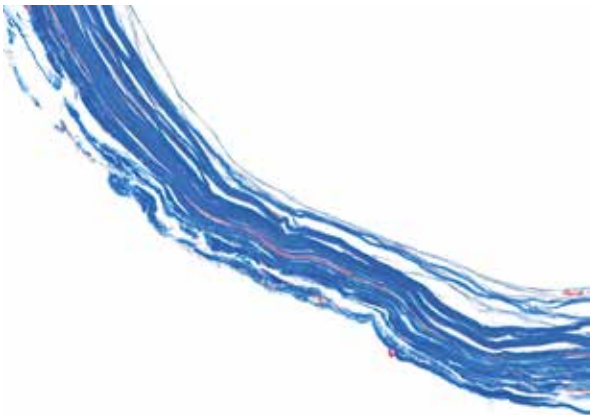

Fig. 8. Aneurysm wall with generalized smooth muscle degeneration (hypocellular wall). Magnification 400×, Mallory trichrome stain.

Statistical analysis

Statistical analyses were performed using the statistical package STATISTICA 13.1 (StatSoft, Inc.) and the R environment [24]. All continuous and ordinal variables are summarized as the mean and standard deviation (SD). Percentages, numerators and denominators are presented for categorical and binary variables. To examine differences between two groups with continuous variables, Student's t-test for independent samples was used. To examine qualitative variables, Fisher's exact test was used. For all calculations, the statistical significance level was $\alpha = 0.05$. *P*-values were unadjusted for multiple comparisons. "PWR" package was used to calculate power for Student's *t*-test for independent samples. Assuming Cohen's d as 0.5, the calculated power was 0.09.

Results

Aneurysm morphology and rupture pressure

Detailed data on age, sex, and cause of death together with the location and characteristics of sIAs are presented in Table I. During pressure-inflation tests, three specimens ruptured at the aneurysm dome (mean maximal dome size: 6.46 ±3.45 mm; mean neck width: 3.12 ±1.11 mm; irregular dome shape: 66.7% of cases). In the other 5 cases (mean maximal dome

Table I. Demographic data and intracranial aneurysm characteristics

Age	Sex	Cause of death	Generalized atherosclerosis[a]	Aneurysm location	Rupture pressure (mmHg)	Rupture site	Irregular shape	MDS (mm)	NW (mm)	IEL	Degenerative changes[b]					Inflammatory infiltration[c]			
											A (%)	B (%)	C (%)	D (%)	E (%)	$CD3^+$ (IL)	$CD3^+$ (Ad)	$CD68^+$ (IL)	$CD68^+$ (Ad)
60	M	Acute myocardial infarction	+	RMCA bif	1321	Artery	+	2.89	2.26	–	0	40	50	10	0	6	0	0	0
60	M	Suicidal hanging	+	LMCA bif	1462	Artery	–	1.84	2.03	+	100	0	0	0	0	0	4	2	1
63	F	Generalized cancer	+	LICA bif	1309	Artery	–	2.39	2.05	–	5	0	0	95	0	2	0	3	0
69	M	Alcohol poisoning	+	ACommA	813	Artery	–	2.72	2.33	–	100	0	0	0	0	0	2	0	2
61	M	Alcohol poisoning	+	LICA bif	1388	Artery	–	2.31	2.70	+	90	0	0	10	0	2	2	0	0
55	F	Pneumonia	+	ACommA	681	Aneurysm	+	10.34	2.82	–	20	20	30	10	20	4	0	0	0
67	M	Suicidal hanging	+	LMCA bif	596	Aneurysm	–	5.32	4.35	–	10	0	0	90	20	2	0	2	0
58	M	Drowning	+	LICA bif	1030	Aneurysm	+	3.73	2.20	–	0	20	20	60	50	8	0	10	0

+ present, – absent, M – male, F – female, R – right, L – left, ACommA – anterior communicating artery, MCA bif – middle cerebral artery bifurcation, ICA bif – internal carotid artery bifurcation, MDS – maximal dome size, NW – neck width, IEL – internal elastic lamina, A – thinned wall with linearly organized smooth muscle cells, B – thickened wall with disorganized smooth muscle cells, C – thickened, hypocellular wall with myointimal hyperplasia, D – extremely thin hypocellular wall, E – region of the hypocellular wall with hyalinization, $CD3^+$ – T lymphocytes, $CD68^+$ – macrophages, IL – inner layers, Ad – adventitia.

[a]The presence of the atherosclerotic plaques within the aorta and coronary arteries found during general autopsy.

[b]The cumulative percentage of degenerative changes within the sIA wall may exceed 100% because of the hyalinization overlapping with type C and D degenerative changes.

[c]The inflammatory infiltration density of T lymphocytes and macrophages in particular layers of the sIA wall is presented as the cell count per standardized grid area, i.e., 0.0625 mm^2.

DH – dome height, DW – dome width, NW – neck width, SD – standard deviation

Fig. 9. Unruptured aneurysm. Discontinuity of internal elastic lamina in the aneurysm wall (arrows). Magnification 100×, Orcein stain.

size: 2.43 ±0.41 mm; mean neck width: 2.27 ±0.27 mm; irregular dome shape: 20% of cases), rupture occurred at the arterial wall. Aneurysms with low wall strength had a significantly higher mean maximal dome size than those with high wall strength ($p = 0.034$). No significant differences between the sIA wall strength categories with regard to neck width and irregular dome shape were observed. The mean sIA rupture pressure was 769 ±230 mmHg, and the average rupture pressure of the arterial wall was 1259 ±256 mmHg. Significantly lower mean rupture pressure was observed for the sIAs than for the arterial wall ($p = 0.035$).

Degenerative changes and inflammation of the aneurysm wall

Internal elastic lamina

All sIAs had preserved or locally fragmented internal elastic lamina (IEL) in the neck area. Atrophy of IEL within the dome was observed in 6 cases (Fig. 9). In the remaining 2 cases (DH ≈ 1 mm), a partially preserved IEL was noted in the dome. sIAs with partially preserved IEL had considerably lower DH as compared to sIAs with atrophy of IEL ($p = 0.028$) (Table II).

Degenerative changes

Several different types of degenerative changes were observed in six of the analysed sIAs. Furthermore,

Table II. Dimensions of intracranial aneurysms in relation to internal elastic lamina preservation

Dimension	Internal elastic lamina				*P*-value
	Absent		Present		
	Mean	SD	Mean	SD	
DH (mm)	2.35	0.63	1.00	0.06	0.03
DW (mm)	3.69	1.50	2.09	0.30	0.20
NW (mm)	2.67	0.86	2.37	0.47	0.66

Table III. Comparison of degenerative change percentages and inflammatory cell infiltration density in relation to aneurysm wall strength

Parameter	Aneurysm wall strength[a]				*P*-value
	Low		High		
	Mean	SD	Mean	SD	
A [%]	10	10	59	51.8	0.167
B [%]	13.3	11.5	8	17.9	0.665
C [%]	16.7	15.3	10	22.4	0.668
D [%]	53.3	40.4	23	40.6	0.345
E [%]	30	17.3	0	0	0.006
$CD3^+$ IL	4.7	3.1	2	2.4	0.220
$CD3^+$ Ad	0	0	1.6	1.7	0.160
$CD68^+$ IL	4	5.3	1	1.4	0.255
$CD68^+$ Ad	0	0	0.6	0.9	0.304

A – thinned wall with linearly organized smooth muscle cells, B – thickened wall with disorganized smooth muscle cells, C – thickened, hypocellular wall with myointimal hyperplasia, D – extremely thin hypocellular wall, E – region of hypocellular wall with hyalinization, $CD3^+$ – T lymphocytes, $CD68^+$ – macrophages, IL – inner layers, Ad – adventitia, SD – standard deviation.

[a]Low wall strength corresponds to aneurysms that ruptured during pressure-inflation tests; high wall strength corresponds to aneurysms that sustained pressurization.

the degree of their advancement tended to increase in the neck-to-dome direction. No significant relations between the percentage of particular types of degenerative changes within the wall and the dimensions of the sIAs were determined ($p > 0.05$). Degenerative changes type B (Figs. 3, 4) and C (Figs. 5, 6) occurred considerably more often in the sIAs with irregular dome shape ($p = 0.002$ for both comparisons). All of the degenerative changes did not significantly differ between groups of sIAs according to the rupture site and AC presence ($p > 0.05$). Nevertheless, in sIAs that ruptured, a significantly higher percentage of degenerative changes corresponding to hyalinization was observed in comparison with sIAs that did not rupture during pressure-inflation tests ($p = 0.01$). Furthermore, regions of hyalinization were more robust within the sIAs wall with AC compared to sIAs without AC ($p = 0.01$). Thus, we distinguished another type E of degenerative changes reflecting regions of hyalinization (Fig. 6, Table III). Cumulative percentage of degenerative changes within the sIAs wall in 2 cases exceeds 100% because of the hyalinization overlapping other types of degenerative changes, i.e. types C and D.

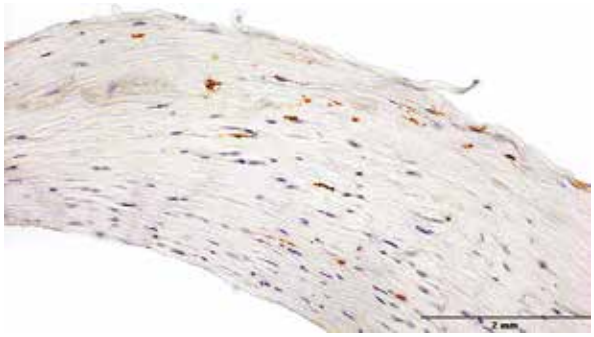

Fig. 10. T-lymphocytes in the aneurysm wall. Magnification 400×, IHC reaction with antibody CD3.

In the last two cases, the dome of the sIA was mainly composed of thin and hypocellular wall – type D degenerative changes (Figs. 7, 8). Compared with that, in sIAs with high wall strength, a significantly higher average percentage of hyalinization (Fig. 6) was observed in sIAs that ruptured during the pressure-inflation tests ($p = 0.006$).

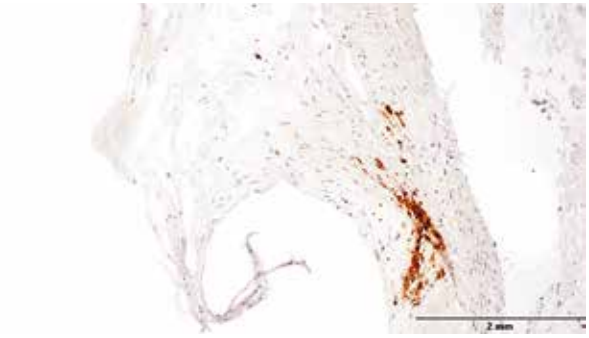

Fig. 11. Macrophages in the aneurysm wall. Magnification 400×, IHC reaction with antibody CD68.

Inflammation

All sIAs showed infiltration of LCA^+, $CD3^+$ and $CD68^+$ cells in the area of both adventitia and inner layers of the wall (Figs. 10, 11, Table I). No significant relations between the infiltration of lymphocytes and macrophages of the wall and dimensions of the sIAs were observed ($p > 0.05$). Furthermore, sIAs did not differ in terms of the degree of inflammation of the wall depending on the rupture site and AC presence ($p > 0.05$). However, compared to regular sIAs, a higher infiltration of $CD3^+$ cells within the inner layers of the wall was determined in the group of sIAs with irregular dome ($p = 0.004$).

Furthermore, in all of the sIAs that ruptured, infiltration of both $CD3^+$ and $CD68^+$ cells within the adventitia was not observed. Nevertheless, the analysed sIAs did not differ in terms of the degree of wall inflammation depending on their wall strength (Table III).

Discussion

Size as a determinant of aneurysm wall strength

The sIA rupture pressure was significantly lower than the pressure for cerebral artery rupture, suggesting a lower strength of the sIA walls that ruptured during the pressure-inflation tests. Robertson *et al*. conducted uniaxial extension tests of unruptured sIAs obtained during surgical clipping. Based on the failure stress values, the authors divided the analysed walls of the sIAs into high- and low-strength categories. On the basis of Laplace's law, the rupture pressure of both sIA categories was estimated. Higher strength sIAs ruptured at pressures ranging from 945 to 3300 mmHg, whereas the rupture pressure of the 2 sIAs with lower failure stress was estimated at 264 and 454 mmHg [21]. In our study, the rupture pressure values of 3 analysed sIAs, equal to 596, 681 and 1030 mmHg, were closer to the values of the lower strength category, confirming the wall instability of the sIAs that ruptured during the pressure-inflation tests. In all other cases of sIA specimens with a perforation at the arterial wall, the dimensions of the dome were < 3 mm.

This is consistent with the findings of previous observational studies. According to the multicentre UCAS Japan study, the rupture risk of sIAs with a dome size equal to 3-4 mm is extremely low but is considerably higher for sIAs measuring ≥ 7 mm [6]. The results of a lifelong Finnish cohort follow-up study showed that in nearly 80% of ruptured sIAs, although they were small at the beginning of the observation period, their dome had increased to ≥ 7 mm at the time of subarachnoid haemorrhage [10]. In our study, even though two of the sIAs that ruptured during pressure-inflation tests were < 7 mm in size, their rupture pressure significantly exceeded the physiological blood pressure values. At the same time, the mean sIA rupture pressure was significantly lower than the average pressure needed for cerebral artery rupture, suggesting ongoing destructive processes weakening the wall of the pressurized sIAs.

Internal elastic lamina degeneration and nascent aneurysm formation

Degradation of the IEL and atrophy of smooth muscle cells in the juxta-apical region of cerebral arterial bifurcations occur first during sIA pathogenesis [15]. In our study, 2 sIAs with the smallest maximal dome size were localized in the juxta-apical region of the middle cerebral artery and the internal carotid artery bifurcation. These nascent sIAs were characterized by the presence of partially preserved, thin and locally fragmented IELs, and degenerative type A changes within the dome.

Healing and destructive processes

According to Laplace's law, intramural stress within the sIA wall is positively correlated with transmural pressure and the dome radius, and negatively correlated with wall thickness. When assuming similar pressure conditions, larger sIAs experience remarkably higher intramural stress than their smaller counterparts with the same wall thickness. Thus, processes leading to wall thickening theoretically increase the sIA wall strength. Such adaptive processes are induced by smooth muscle cell dedifferentiation from a contractile to a pro-matrix remodelling phenotype. Dedifferentiated smooth muscle cells migrate toward the intima, proliferate, secrete matrix metalloproteinases and synthesize extracellular matrix proteins to form myointimal hyperplasia increasing the strength of the wall [4].

Such positive wall remodelling during sIA formation may explain counterintuitive finding that sIAs < 3 mm presented higher wall strength than the wall of adjacent cerebral arteries.

Histological analysis revealed that sIAs with low wall strength were characterized by regions of wall hyalinization. The essence of hyalinization is the increased penetration of blood serum into the vessel wall (mainly the tunica media). This causes damage to the smooth muscle cells and conversion to an eosinophilic homogeneous mass. In the area of hyalinization, the structure of the medial membrane becomes blurred, which impairs autoregulation, reduces the flexibility of the wall and most likely makes it more prone to rupture.

Moreover, inflammatory cell infiltration within the adventitia was exclusively absent among sIAs that ruptured during the experiments. Such adventitial infiltration may occur during the early stages of sIA formation. The results of the study by Koseki *et al*. indicate that mechanical stretching of the bulged-out and thinned arterial wall may induce the expression of monocyte chemoattractant protein 1 (MCP1) in adventitial fibroblasts, initiating macrophage infiltration within the adventitia of nascent sIAs [11]. Next, inflammatory cells elicit degradation of collagen, which is the main load-bearing material of sIAs. Because stiff collagen fibres are amenable to slight deformations prior to failure [21], sIA growth is associated with constant processes of collagen degradation and synthesis [3]. In our study, the average rupture pressure of sIAs was lower than the mean rupture pressure of the middle cerebral artery adventitia, which is mainly composed of collagen [17]. Thus, hyalinization may represent regions of collagen degradation and may be responsible for both the growth and rupture of sIAs.

Aneurysm phenotypes and clinical implications

Meng *et al*. distinguished 3 sIA phenotypes based on different hypothetical pathological mechanisms. Type I refers to small, spherical and thin-walled sIAs. Histologically, their wall is characterized by generalized smooth muscle cell degeneration with absent or minor inflammatory cell infiltration [14]. These specific aneurysms may enlarge in a short time or rupture soon after formation [22]. In our study, two of the sIAs with a marked predominance of type D degenerative changes resembled this sIA phenotype. Type II sIAs are characterized by atherosclerotic walls with regions of myointimal hyperplasia, organized thrombosis and inflammatory cell infiltration. These sIAs are large and irregular and may develop over a long period, showing irregular growth with an increased and decreased risk of rupture occurring interchangeably [14]. If destructive processes, leading to the weakening of the sIA wall, prevail over adaptive processes, rupture of the sIA occurs [9]. The most common type is medium-sized type III, which is referred to as a combination type. In our study, this sIA phenotype was observed in four cases, and all types of degenerative changes were present within their walls. Furthermore, a tendency toward the occurrence of more advanced degenerative changes, such as type C or D, from the neck to the apex of the dome was observed. Wall hyalinization representing regions of low wall strength was present in both type I and III sIAs analysed, implying that rupture may occur independently of the sIA size. Thus, rupture risk evaluation is still a challenging issue.

A recent longitudinal study concerning vessel wall magnetic resonance imaging (MRI) of unruptured sIAs revealed that aneurysm wall enhancement (AWE) might play a role as a potential marker of an increased risk of sIA growth or rupture [25]. Interestingly, our findings are in concordance with the results of histopathological studies of sIAs with AWE. Among our sIA specimens, hyalinization, reflecting wall destructive processes, seems to be associated with macrophage infiltration. Similarly, Shimonaga *et al*. found that abundant macrophage infiltration corresponded to AWE on vessel wall MRI [23]. The reported decrease in AWE after administration of acetylsalicylic acid [20], which stabilizes the sIA wall by reducing macrophage infiltration [5], further confirms the important role of macrophages in destructive processes leading to sIA wall instability. Complex diagnostic tools utilizing MRI and AWE with concomitant quantitative analysis of serum levels of matrix metalloproteinases [7] responsible for collagen degradation could clarify more precisely which group of patients would benefit from invasive preventive treatment of especially small, unruptured sIAs.

Limitations

Our study was limited due to the small number of analysed sIA specimens measuring < 7 mm in size, which may lead to discrepancies regarding the impact of inflammatory infiltration on sIA wall strength. Contrary to the literature data [4,8,16], in our study, the rupture site of analysed sIA specimens was not related to inflammatory infiltration. Second, in the current study, effect sizes were not high and the examined sample size was low, therefore the power of the statistical test was low. As it is a pilot study, it should be replicated with a larger sample size. Third, pressure-inflation tests were conducted on sIA specimens collected from deceased patients within 36 hours of their death. Thus, the processes of autolysis may have affected the analysis of the strength and structure of the sIA wall. Finally, the sIA specimens were subjected

to supraphysiological pressures during the pressure-inflation tests. Compared to observations in unruptured sIAs, increased de-endothelialization with concomitant fresh thrombosis covering the luminal surface of the dome was observed in ruptured sIAs [4]. In our study, neither fresh luminal thrombosis nor endothelial cells were observed during the initial microscopic analysis of the sIAs. We can infer that thin and sensitive layers of endothelial cells and any potential fresh luminal thrombosis were washed out during our experiments.

Conclusions

Unruptured sIAs may sustain very high supraphysiological pressures until they rupture. Moreover, sIAs with a dome size < 3 mm presented higher wall strength than the strength of the parent artery and all of its branches. Larger sIAs ruptured during the pressure-inflation tests, supporting the observation that sIA rupture risk increases with increasing dome size. The only distinctive histological feature of sIAs with low wall strength was the presence of hyalinization corresponding to the regions of ongoing destructive processes weakening the aneurysmal wall. At the same time, inflammatory cell infiltration was present in all sIAs regardless of their wall strength, indicating that inflammation is related to various stages of sIA development. However, infiltration of both lymphocytes and macrophages within the adventitia was present solely among sIAs < 3 mm in size, suggesting that adventitial inflammation may occur at the initial stages of sIA formation. Further experiments conducted on a higher number of sIAs may provide better insights into the exact role of inflammation in eliciting destructive processes leading to sIA rupture.

Acknowledgments

We would like to thank American Journal Experts (https://www.aje.com) for English language editing.

Disclosure

The authors report no conflict of interest.

References

1. Darsaut TE, Findlay JM, Magro E, Kotowski M, Roy D, Weill A, Bojanowski MW, Chaalala C, Iancu D, Lesiuk H, Sinclair J, Scholtes F, Martin D, Chow MM, O'Kelly CJ, Wong JH, Butcher K, Fox AJ, Arthur AS, Guilbert F, Tian L, Chagnon M, Nolet S, Gevry G, Raymond J. Surgical clipping or endovascular coiling for unruptured intracranial aneurysms: a pragmatic randomised trial. J Neurol Neurosurg Psychiatry 2017; 88: 663-668.
2. Das S, Valyi-Nagy T. Multiple cerebral fusiform aneurysms involving the posterior and anterior circulation including the anterior cerebral artery: a case report. Folia Neuropathol 2017; 55: 73-76.
3. Etminan N, Dreier R, Buchholz BA, Beseoglu K, Bruckner P, Matzenauer C, Torner JC, Brown RD, Jr., Steiger HJ, Hanggi D, Macdonald RL. Age of collagen in intracranial saccular aneurysms. Stroke 2014; 45: 1757-1763.
4. Frösen J, Piippo A, Paetau A, Kangasniemi M, Niemela M, Hernesniemi J, Jaaskelainen J. Remodeling of saccular cerebral artery aneurysm wall is associated with rupture: histological analysis of 24 unruptured and 42 ruptured cases. Stroke 2004; 35: 2287-2293.
5. Hasan DM, Chalouhi N, Jabbour P, Dumont AS, Kung DK, Magnotta VA, Young WL, Hashimoto T, Richard Winn H, Heistad D. Evidence that acetylsalicylic acid attenuates inflammation in the walls of human cerebral aneurysms: preliminary results. J Am Heart Assoc 2013; 2: e000019.
6. Investigators UJ, Morita A, Kirino T, Hashi K, Aoki N, Fukuhara S, Hashimoto N, Nakayama T, Sakai M, Teramoto A, Tominari S, Yoshimoto T. The natural course of unruptured cerebral aneurysms in a Japanese cohort. N Engl J Med 2012; 366: 2474-2482.
7. Jin D, Sheng J, Yang X, Gao B. Matrix metalloproteinases and tissue inhibitors of metalloproteinases expression in human cerebral ruptured and unruptured aneurysm. Surg Neurol 2007; 68 Suppl 2: S11-16; discussion S16.
8. Kataoka K, Taneda M, Asai T, Kinoshita A, Ito M, Kuroda R. Structural fragility and inflammatory response of ruptured cerebral aneurysms. A comparative study between ruptured and unruptured cerebral aneurysms. Stroke 1999; 30: 1396-1401.
9. Koffijberg H, Buskens E, Algra A, Wermer MJ, Rinkel GJ. Growth rates of intracranial aneurysms: exploring constancy. J Neurosurg 2008; 109: 176-185.
10. Korja M, Lehto H, Juvela S. Lifelong rupture risk of intracranial aneurysms depends on risk factors: a prospective Finnish cohort study. Stroke 2014; 45: 1958-1963.
11. Koseki H, Miyata H, Shimo S, Ohno N, Mifune K, Shimano K, Yamamoto K, Nozaki K, Kasuya H, Narumiya S, Aoki T. Two Diverse hemodynamic forces, a mechanical stretch and a high wall shear stress, determine intracranial aneurysm formation. Transl Stroke Res 2020; 11: 80-92.
12. Lee GJ, Eom KS, Lee C, Kim DW, Kang SD. Rupture of very small intracranial aneurysms: incidence and clinical characteristics. J Cerebrovasc Endovasc Neurosurg 2015; 17: 217-222.
13. Li J, Shen B, Ma C, Liu L, Ren L, Fang Y, Dai D, Chen S, Lu J. 3D contrast enhancement-MR angiography for imaging of unruptured cerebral aneurysms: a hospital-based prevalence study. PLoS One 2014; 9: e114157.
14. Meng H, Tutino VM, Xiang J, Siddiqui A. High WSS or low WSS? Complex interactions of hemodynamics with intracranial aneurysm initiation, growth, and rupture: toward a unifying hypothesis. AJNR Am J Neuroradiol 2014; 35: 1254-1262.
15. Meng H, Wang Z, Hoi Y, Gao L, Metaxa E, Swartz DD, Kolega J. Complex hemodynamics at the apex of an arterial bifurcation induces vascular remodeling resembling cerebral aneurysm initiation. Stroke 2007; 38: 1924-1931.
16. Morel S, Diagbouga MR, Dupuy N, Sutter E, Braunersreuther V, Pelli G, Corniola M, Gondar R, Jagersberg M, Isidor N, Schaller K, Bochaton-Piallat ML, Bijlenga P, Kwak BR. Correlating Clinical Risk Factors and Histological Features in Ruptured and Unruptured Human Intracranial Aneurysms: The Swiss AneuX Study. J Neuropathol Exp Neurol 2018; 77: 555-566.
17. Piechna A, Lombarski L, Ciszek B, Cieslicki K. Experimental determination of rupture pressure and stress of adventitia of human middle cerebral arteries. Int J Stroke 2017; 12: 636-640.

18. Rafałowska J. Developmental failures of blood vessels within central nervous system. Folia Neuropathol 1995; 33: 201-206.
19. Rinkel GJ. Medical management of patients with aneurysmal subarachnoid haemorrhage. Int J Stroke 2008; 3: 193-204.
20. Roa JA, Zanaty M, Ishii D, Lu Y, Kung DK, Starke RM, Torner JC, Jabbour PM, Samaniego EA, Hasan DM. Decreased contrast enhancement on high-resolution vessel wall imaging of unruptured intracranial aneurysms in patients taking aspirin. J Neurosurg 2020; 134: 902-908.
21. Robertson AM, Duan X, Aziz KM, Hill MR, Watkins SC, Cebral JR. Diversity in the strength and structure of unruptured cerebral aneurysms. Ann Biomed Eng 2015; 43: 1502-1515.
22. Sato K, Yoshimoto Y. Risk profile of intracranial aneurysms: rupture rate is not constant after formation. Stroke 2011; 42: 3376-3381.
23. Shimonaga K, Matsushige T, Ishii D, Sakamoto S, Hosogai M, Kawasumi T, Kaneko M, Ono C, Kurisu K. Clinicopathological insights from vessel wall imaging of unruptured intracranial aneurysms. Stroke 2018; 49: 2516-2519.
24. Team RC. R: A language and environment for statistical computing. Vienna, Austria 2013.
25. Vergouwen MDI, Backes D, van der Schaaf IC, Hendrikse J, Kleinloog R, Algra A, Rinkel GJE. Gadolinium enhancement of the aneurysm wall in unruptured intracranial aneurysms is associated with an increased risk of aneurysm instability: a follow-up study. AJNR Am J Neuroradiol 2019; 40: 1112-1116.